3-D Full-Vectorial Analysis of Strong Optical Waveguide Discontinuities Using Pade Approximants

Husain A. Jamid and Md. Zahed M. Khan

***Abstract*—A full-vectorial 3-D numerical method applicable to high-index contrast optical waveguide discontinuities is presented. Rigorous treatment of the longitudinal boundary condition is incorporated in the formulation. The square root of the characteristic matrix is approximated using Padé approximants which results in an efficient implementation. The biconjugate gradient stabilized method is utilized to iteratively calculate the reflected and transmitted fields. A preconditioner is proposed which results in reduced number of iterations. The proposed method is applied to various optical waveguide facets exhibiting strong transverse and longitudinal refractive index discontinuities. In all cases, the modal reflectivities of the fundamental TE-Like and TM-Like modes are calculated for both the full-vectorial and the semi-vectorial formulations. Significant difference in the calculated modal reflectivity is seen between the full and semi-vectorial models. The error in the power balance remains low in the full-vectorial case irrespective of the waveguide dimensions. However, in the semi-vectorial case, the error in the power balance is found to increase when the waveguide width is reduced.**

***Index Terms*—Full-vectorial methods, Padé approximants, preconditioner, 3-D waveguides, waveguide facet, waveguide discontinuities.**

I. Introduction

OPTICAL waveguide discontinuities have been the subject of intense research interest in the past several years. These discontinuities occur in a wide range of active and passive optical devices. The previously reported work has been based on 2-D as well as 3-D models of the waveguide discontinuity. Various numerical methods have been applied in the analysis of waveguide facets. This includes for instance, the finite-element method (FEM) [1], [2], the finite-difference time-domain method (FDTD) [3], [4], the free space radiation mode (FSRM) method [5], the mode matching method (MMM) [6], [7], methods that utilize radiation modes [8], [9], the method of lines (MoL) [10]–[13], and the bidirectional beam propagation method (bidirectional BPM) [14]–[23]. In recent years, the 2-D version of the waveguide facet problem became trivial. This is largely due to the development of various numerical methods, some of which are very efficient, and the advent of fast processors. However, extension of these methods from the 2-D to the 3-D model generally remains nontrivial. The major and common reason for this difficulty is the resulting large and in some cases prohibitive increase in processing time and memory requirements, especially for full-vector-based models. Another reason has to do with the level of theoretical/numerical difficulties encountered in extending a particular method to the 3-D case.

An efficient Bi-directional MoL-BPM based numerical method which utilizes Padé approximants of the square root operator has been reported in the literature for single [14]–[16] and multiple [17]–[21] abrupt 2-D longitudinal waveguide discontinuities. In its basic form, this method can correctly account only for guided modes and does not account correctly for evanescent modes. The use of branch cut rotation allows this method to account for both guided and evanescent modes simultaneously [15], [18]–[20]. It is well-known that highly evanescent modes are excited at strong longitudinal discontinuities. The ability of this method to account for highly evanescent modes, with no extra numerical effort, makes it equally suitable for the treatment of 3-D waveguide facets with weak or strong index discontinuities. This is a highly desirable property to have in a numerical method, especially in the case of 3-D modeling. Some numerical methods lack this feature. For instance, the MMM is known to be efficient in the treatment of weak 3-D longitudinal discontinuities, because in this case only guided modes need to be accounted for. However, for strong 3-D longitudinal discontinuities, in which case highly evanescent modes must be accounted for, the MMM becomes prohibitively inefficient. The bidirectional MoL-BPM has previously been applied to calculate the 3-D waveguide facet reflectivity [22], [23]. While the earlier work [22] does not utilize Padé approximants of the square root operator, the later one [23] is based on Padé approximants with complex coefficients. However, both of these reported works have been based on the semi-vectorial formulation. To the best of our knowledge, extension of the bidirectional MoL-BPM that utilizes Padé approximants with branch cut rotation and based on the more realistic 3-D full-vectorial model has not been reported in the literature. Our own experience with this problem suggests that the lack of reported work may be due to difficulties encountered in accounting accurately for the full-vectorial nature of the field and in the slow or lack of convergence of the numerical solution.

One aim of this work is to present an approach for extending the above-mentioned method to the 3-D full-vectorial rather than the approximate semi-vectorial formulation. A rigorous longitudinal boundary condition which accounts for the continuity of all transverse electric and magnetic field components at an abrupt longitudinal discontinuity will also be utilized in

Manuscript received September 15, 2006; revised December 22, 2006. This work was supported in part by King Fahd University of Petroleum and Minerals, Dhahran, Saudi Arabia.

H. A. Jamid is with the Electrical Engineering Department, King Fahd University of Petroleum and Mineral, Dhahran 31261, Saudi Arabia (e-mail: hajamed@kfupm.edu.sa).

Md. Z. M. Khan is with the Electrical and Electronics Engineering Technology Department, Hafr Al-Batin Community College, King Fahd University of Petroleum and Minerals, Hafr Al-Batin, 31991 Saudi Arabia (e-mail: zahedmk@yahoo.co.in).

Digital Object Identifier 10.1109/JQE.2007.893007

the numerical method. In addition, a proposed preconditioner will be presented which enhances the efficiency of the numerical calculations by reducing the number of iterations required for convergence. Finally, the 3-D facet reflectivity of a number of waveguide structures exhibiting strong transverse and longitudinal index discontinuities will be calculated by the proposed method. The facet reflectivity results based on the semi-vectorial and full-vectorial assumptions will then be compared to highlight the difference in the predictions of these two models.

II. Theory

The present work is based on the transverse magnetic field (H_x, H_y) formulation. This formulation has been chosen because it is known not to generate spurious modes [24], [25] and also because the transverse magnetic field components H_x and H_y are continuous at material discontinuities. It is also known that the remaining electromagnetic components of the vectorial field can be expressed in terms of the transverse magnetic field components. The theoretical framework of the present approach is as follows. First, the H-field formulation is developed, then a suitable relationship that expresses the discretized transverse electric field components in terms of the discretized transverse magnetic field components is derived. Finally, the longitudinal boundary condition is rigorously enforced, utilizing the continuity of all four transverse field components at an abrupt longitudinal discontinuity.

A. Transverse H-Field Formulation

In a locally homogeneous medium with refractive index n, the transverse magnetic field satisfies the 3-D wave equation

$$\frac{\partial^2 H}{\partial x^2}+\frac{\partial^2 H}{\partial y^2}+\frac{\partial^2 H}{\partial z^2}+k_0^2 n^2 H=0 \tag{1}$$

where H represents either H_x or H_y and $k_0=2\pi/\lambda$ is the free space wave number. Equation (1) is first discretized in the transverse direction (x, y) and then solved analytically in the longitudinal direction (z). A discrete form of (1) which accounts for the transverse boundary conditions and transverse magnetic field coupling at abrupt transverse discontinuities has been reported in [25]. It results in the following matrix second-order ordinary differential equation:

$$\frac{d\overline{H}}{dz^2}+\overline{Q}^2\overline{H}=\overline{0} \tag{2}$$

where $\overline{H}=\begin{pmatrix}\overline{H}_x\\ \overline{H}_y\end{pmatrix}$. The column vectors $\overline{H}_x$ and $\overline{H}_y$ contain the discretized values of H_x and H_y in the transverse direction, respectively. For a computational window containing $M\times N$ samples in the x and y directions, respectively, the dimension of each of the column vectors $\overline{H}_x$ and $\overline{H}_y$ is $MN\times 1$ and thus the dimension of $\overline{H}$ is $2MN\times 1$. The square matrix $\overline{Q}^2$ is given by [25]

$$\overline{Q}^2=\begin{pmatrix}\overline{A}_{XX} & \overline{A}_{XY}\\ \overline{A}_{YX} & \overline{A}_{YY}\end{pmatrix}. \tag{3}$$

The dimension of each of the square submatrices $\overline{A}_{XX}$, $\overline{A}_{XY}$, $\overline{A}_{YX}$, and $\overline{A}_{YY}$ is $MN\times MN$. The reader is referred to [25] for details necessary for the construction of these four submatrices. It is noteworthy to mention that the submatrices $\overline{A}_{XY}$ and $\overline{A}_{YX}$ account for transverse magnetic field coupling. The general solution of (2) is given by

$$\overline{H}=e^{j\overline{Q}z}\overline{A}+e^{-j\overline{Q}z}\overline{B}. \tag{4}$$

The square matrices $e^{+j\overline{Q}z}$ and $e^{-j\overline{Q}z}$ account for the forward and backward fields, respectively.

B. Transverse E-Field in Terms of Transverse H-Field

In order to rigorously satisfy the *longitudinal* boundary condition, accurate expressions for the transverse electric field components E_x and E_y (in terms of transverse magnetic field components H_x and H_y) are required. These expressions can easily be derived from Maxwell's equations, assuming a locally uniform medium, and are given by the following integral expressions:

$$E_x=\frac{-j\sqrt{\mu_0/\varepsilon_0}}{k_0}\frac{1}{n^2}\left[\int\left(\frac{\partial^2 H_y}{\partial y^2}+\frac{\partial^2 H_x}{\partial x\partial y}+\frac{\partial^2 H_y}{\partial z^2}\right)dz\right] \tag{5}$$

$$E_y=\frac{j\sqrt{\mu_0/\varepsilon_0}}{k_0}\frac{1}{n^2}\left[\int\left(\frac{\partial^2 H_x}{\partial x^2}+\frac{\partial^2 H_y}{\partial y\partial x}+\frac{\partial^2 H_x}{\partial z^2}\right)dz\right]. \tag{6}$$

The longitudinal boundary condition requires continuity of the transverse magnetic and transverse electric field components. Equations (5) and (6) will be utilized to insure continuity of the transverse electric field components at an abrupt longitudinal discontinuity.

Prior to discretization of (5) and (6), they are first combined into the following single relation:

$$\begin{pmatrix}E_y\\ -E_x\end{pmatrix}=\xi\frac{1}{n^2}\left\{\begin{pmatrix}\frac{\partial^2}{\partial x^2} & \frac{\partial^2}{\partial y\partial x}\\ \frac{\partial^2}{\partial x\partial y} & \frac{\partial^2}{\partial y^2}\end{pmatrix}+\frac{\partial^2}{\partial z^2}\right\}\int\begin{pmatrix}H_x\\ H_y\end{pmatrix}dz \tag{7}$$

where $\xi=j\sqrt{\mu_0/\varepsilon_0}/k_0$. Note that in (7), the order of the integral and differential operators have been interchanged, which is allowable in a locally homogeneous medium. Discretization of (7) in the transverse dimension leads to the following matrix relation:

$$\overline{E}=\xi\overline{N}^{-2}\left(\overline{O}+\frac{d^2}{dz^2}\right)(j\overline{Q})^{-1}\overline{H} \tag{8}$$

where $\overline{E}=(\overline{E}_y \ -\overline{E}_x)^T$ is a column vector with the same dimension as $\overline{H}$. The $MN\times 1$ column vectors $\overline{E}_x$ and $\overline{E}_y$ contain the discretized values of E_x and E_y, respectively. In addition, the dimension of each of the square matrices $\overline{N}^2$ and $\overline{O}$ is $2MN\times 2MN$. The matrices $\overline{N}^2$ and $\overline{O}$ respectively contain the discrete values of the square of the refractive index and the discrete values of the transverse differential operators. The integral operator in (7) has been replaced with the square matrix operator $(j\overline{Q})^{-1}$ assuming a *forward* propagating field. For the backward field, the same integral operator is replaced by $(-j\overline{Q})^{-1}$. Next,

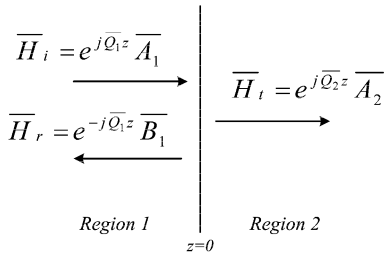

Fig. 1. Incident, reflected, and transmitted fields at an abrupt longitudinal discontinuity located at $z = 0$.

using (2), the longitudinal differential operator d^2/dz^2 in (8) is replaced by $-\overline{Q}^2$ which results in the following relation:

$$\overline{E} = \xi \overline{N}^{-2}(\overline{O} - \overline{Q}^2)(j\overline{Q})^{-1}\overline{H}. \tag{9}$$

Although the longitudinal differential operator d^2/dz^2 in (8) does not *explicitly* contain coupling terms of the transverse magnetic field components at transverse boundaries, it however *implicitly* does. This can easily be seen by examining (2) and (3). Therefore, the use of (2) to replace d^2/dz^2 in (8) is necessary to correctly account for transverse magnetic field coupling at transverse boundaries. Although the two operators $\overline{O}$ and $\overline{Q}^2$ in (9) can in principle be applied separately, various numerical experiments show that application of these operators separately may lead to numerical instabilities. The origin of this instability is due to the discontinuous nature of the spatial second derivates of the transverse magnetic field components at transverse boundaries, which becomes more pronounced in the case of strong transverse material discontinuities. These numerical instabilities can be avoided by combining the matrix operators $\overline{O}$ and $\overline{Q}^2$ into the *single* operator $\overline{F} = (\overline{O} - \overline{Q}^2)$, leading to the relationship

$$\overline{E} = \xi \overline{N}^{-2}\overline{F}(j\overline{Q})^{-1}\overline{H}. \tag{10}$$

C. Formulation of the Longitudinal Boundary Condition

Fig. 1 shows an abrupt longitudinal boundary located at $z = 0$. Region 1, contains the incident and reflected fields and region 2 contains the transmitted field. The incident, reflected and transmitted magnetic fields are, respectively, $\overline{H}_i = e^{j\overline{Q}_1 z}\overline{A}_1$, $\overline{H}_r = e^{-j\overline{Q}_1 z}\overline{B}_1$, and $\overline{H}_t = e^{j\overline{Q}_2 z}\overline{A}_2$. Using (4) and (10) and enforcing continuity of the transverse electric and magnetic fields at $z = 0$ results in the following relations:

$$\overline{A}_1 + \overline{B}_1 = \overline{B}_2 \tag{11}$$

$$\overline{N}_1^{-2}\overline{F}_1\overline{Q}_1^{-1}\overline{A}_1 - \overline{N}_1^{-2}\overline{F}_1\overline{Q}_1^{-1}\overline{B}_1 = \overline{N}_2^{-2}\overline{F}_2\overline{Q}_2^{-1}\overline{B}_2 \tag{12}$$

Equations (11) and (12) are then used to relate the reflected $(\overline{B}_1)$ and transmitted $(\overline{A}_2)$ magnetic fields to the incident $(\overline{A}_1)$ magnetic field

$$\left(\overline{N}_1^{-2}\overline{F}_1\overline{Q}_1^{-1} + \overline{N}_2^{-2}\overline{F}_2\overline{Q}_2^{-1}\right)\overline{B}_1 = \left(\overline{N}_1^{-2}\overline{F}_1\overline{Q}_1^{-1} - \overline{N}_2^{-2}\overline{F}_2\overline{Q}_2^{-1}\right)\overline{A}_1 \tag{13}$$

$$\left(\overline{N}_1^{-2}\overline{F}_1\overline{Q}_1^{-1} + \overline{N}_2^{-2}\overline{F}_2\overline{Q}_2^{-1}\right)\overline{A}_2 = 2\overline{N}_1^{-2}\overline{F}_1\overline{Q}_1^{-1}\overline{A}_1. \tag{14}$$

The square matrix $\overline{Q}$ in (13) and (14) is calculated using Padé approximation of the square root operator [15], [16], [19], [20], [23], [26]

$$\overline{Q} = \gamma^{-\frac{1}{2}}\sqrt{\overline{I} + \overline{X}} = \gamma^{-\frac{1}{2}}\prod_{k=1}^{p}\frac{\overline{I} + a_k^{(p)}\overline{X}}{\overline{I} + b_k^{(p)}\overline{X}} \tag{15}$$

where $\overline{I}$ is the identity matrix, the square matrix $\overline{X} \equiv \gamma\overline{Q}^2 - \overline{I}$ and γ is a complex scalar used for the purpose of branch-cut rotation [15], [18], [19]. The parameter p is Padé order, which is taken to be 4 throughout this work, unless otherwise stated. Closed form expressions for the Padé primes $a_k^{(p)}$ and $b_k^{(p)}$ corresponding to the square root operator have been reported in [20].

D. Proposed Preconditioner

The well-known biconjugate gradient stabilized method (Bi-CGSTAB) has been previously utilized to iteratively calculate the reflected and transmitted fields at an abrupt 2-D waveguide facet [16]. In the present work, the Bi-CGSTAB will be used in tandem with (13) and (14) to iteratively calculate the reflected $(\overline{B}_1)$ and transmitted $(\overline{A}_2)$ fields. However, these equations need to be preconditioned when used in tandem with Bi-CGSTAB, otherwise the performance of BI-CGSTAB may deteriorate, leading to an unacceptably large number of iterations or even failure to converge. Previously reported preconditioners [16], [21], [23], [26] are not suitable for the present formulation. This is due mainly to the full-vector nature of the present problem. A proposed preconditioner suitable for the present formulation is given by the following expression:

$$\overline{P} = (2\overline{I} + 0.5\overline{X}_{\text{avg}})^{-1}(\overline{I} + 0.75\overline{X}_{\text{avg}})(\overline{N}^{-2}\overline{F})_{\text{avg}} \tag{16}$$

where $\overline{X}_{\text{avg}} = 0.5(\overline{X}_1 + \overline{X}_2)$ and $(\overline{N}^{-2}\overline{F})_{\text{avg}} = 0.5(\overline{N_1}^{-2}\overline{F_1} + \overline{N_2}^{-2}\overline{F_2})$. Equation (16) is based on first-order Padé approximant of the square root operator and averaging of the matrix operators. This equation gives a crude approximation to the inverse of the matrix $(\overline{N}_1^{-2}\overline{F}_1\overline{Q}_1^{-1} + \overline{N}_2^{-2}\overline{F}_2\overline{Q}_2^{-1})$ appearing on the left-hand side of (13) and (14). Derivation of (16) will not be reported in this work. To obtain a preconditioned system, the above preconditioner $\overline{P}$ is left-multiplied by (13) and (14).

Although (13) and (14) were obtained assuming a full-vectorial formulation, these equations can also be applied to obtain the results for the semi-vectorial model, as a special case. For the semi-vectorial TM-like model, $\overline{H}$ and $\overline{Q}^2$ are reduced to $\overline{H}_X$ and $\overline{A}_{XX}$, respectively. The square matrices $\overline{N}^2$ and $\overline{O}$ each will now have a reduced dimension of $MN \times MN$. The matrix $\overline{O}$ in this case does not contain any coupling terms. A similar arrangement is applicable in the TE-like semi-vectorial case. Hence, in this manner a unified numerical approach is available for the semi-vectorial and full-vectorial formulations.

III. Numerical Results

The numerical method developed in the previous section will be used to calculate the facet reflectivities of the three waveguide structures shown in Fig. 2, where it is assumed that the transmission medium is air. These waveguides are the buried waveguide Fig. 2(a), channel waveguide suspended in air Fig. 2(b)

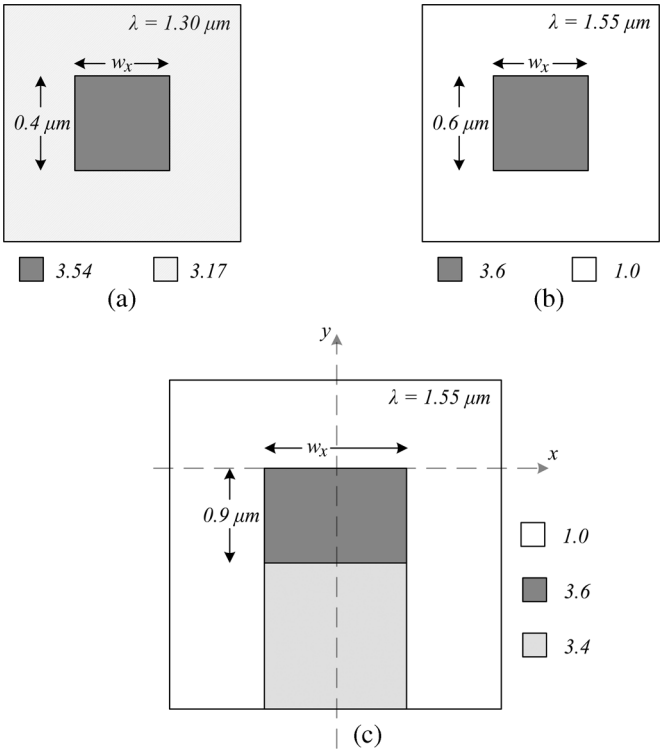

Fig. 2. Optical waveguide structures. (a) Buried waveguide. (b) Waveguide suspended in air. (c) Channel waveguide.

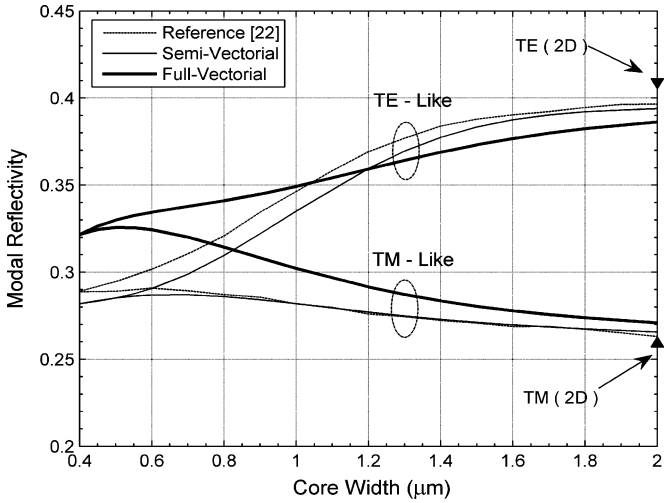

Fig. 3. Calculated TE-Like and TM-Like fundamental mode facet reflectivities corresponding to the waveguide structure shown in Fig. 2(a). The operating wavelength is $\lambda = 1.30\ \mu$m.

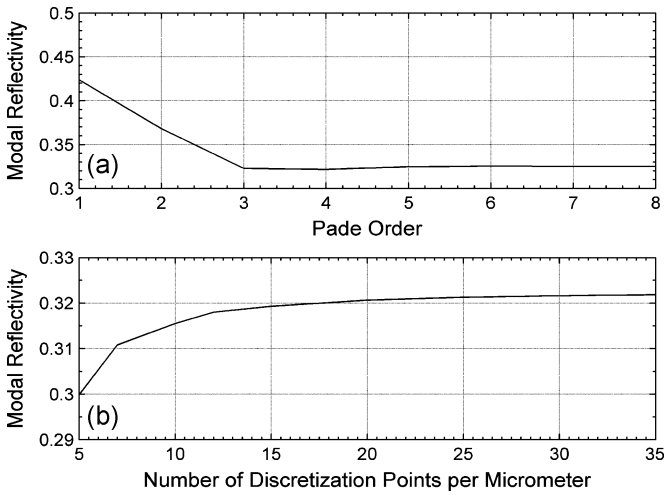

Fig. 4. Calculated full-vectorial reflectivity of the fundamental TE-Like mode as a function of (a) Padé order and (b) transverse mesh density.

and the raised channel waveguide Fig. 2(c). The *fundamental* TE-Like (TE_{00}) and TM-Like (TM_{00}) modes are assumed to be incident on the waveguide facet *throughout* this work. For each of these waveguides, the *modal* facet reflectivity (the ratio of the reflected modal power to incident modal power) will be calculated based on both the semi-vectorial and full-vectorial models. Comparisons of the results of these two models will be presented in the following sections. A perfectly matched absorbing layer (PML) based on transformation of space to the complex domain [27] has been incorporated in the numerical procedure in order to absorb the radiative field.

A. Buried Waveguide

The core of the buried waveguide shown in Fig. 2(a) is assumed to have the refractive index $n_{\text{core}} = 3.54$. The core is surrounded on all sides by a cladding material with the refractive index $n_{\text{clad}} = 3.17$. The core thickness is fixed to 0.4 μm, while the core width w_x is varied. The operating wavelength is $\lambda = 1.30\ \mu$m. Fig. 3 shows the variation of the modal reflectivity as a function of w_x. The curves show the calculated modal reflectivity based on the semi-vectorial and the full-vectorial formulations for the fundamental TE-Like and TM-Like modes. In all cases, it is seen that the modal reflectivity approaches the 2-D results when the waveguide becomes sufficiently wide. The calculated semi-vectorial results are generally in good agreement with those of reference [22], which are also based on a semi-vectorial assumption. The calculated modal reflectivities of the TE-Like and TM-Like modes based on the full-vectorial formulation become substantially higher than the semi-vectorial results when the waveguide width decreases. It is interesting to note that for a core width of $w_x = 0.4\ \mu$m (square waveguide), the TE-Like and TM-Like modes become degenerate giving identical values of the modal reflectivity.

Fig. 4 shows convergence of the calculated full-vectorial reflectivity of the fundamental TE-Like mode corresponding to $w_x = 0.4\ \mu$m for sufficiently large values of Padé order and transverse mesh density. As seen in Fig. 4(a), the calculated results start to converge at Padé order 3. The results shown in Fig. 4(b) have been obtained using the *same* mesh density in the x and y directions. For this particular case, the calculated modal reflectivity is seen to convergence at approximately 25 points/micrometer.

The calculated results shown in Fig. 3 corresponding to $w_x = 0.4\ \mu$m utilize a mesh density of 30 sample points per micrometer in the x and y directions. This corresponds to a transverse computational window (including the PML) with a total of 82 sample points in both the x and y directions. For the full-vectorial case, this results in a sparse square matrix dimension of 13448. The full-vectorial modal reflectivity of

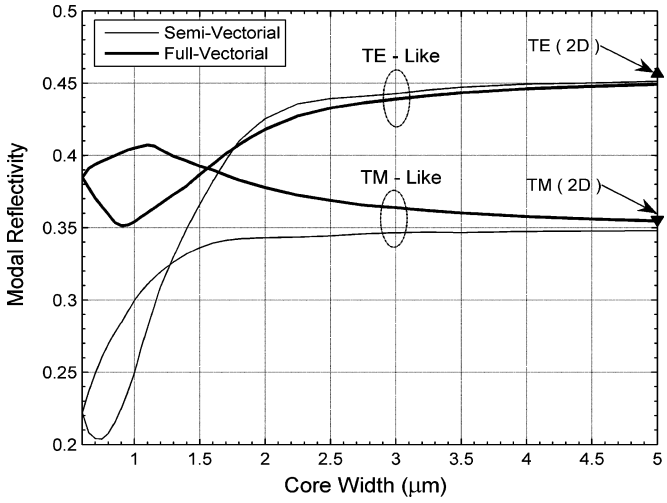

Fig. 5. Calculated TE-Like and TM-Like fundamental mode facet reflectivities corresponding to the waveguide structure shown in Fig. 2(b). The operating wavelength is $\lambda = 1.55$ μm.

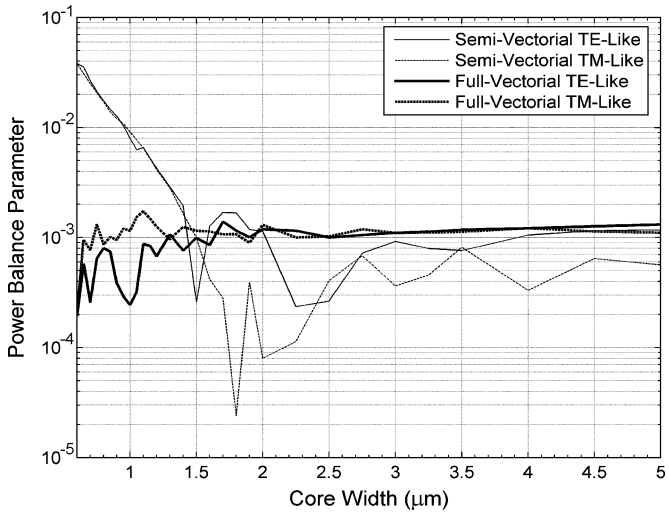

Fig. 6. Variation of the power balance parameter with waveguide width corresponding to the waveguide structure shown in Fig. 2(b).

the fundamental TE-Like mode corresponding to $w_x = 0.4$ μm has been calculated with and without preconditioning. For the preconditioned system, Bi-CGSTAB requires nine iterations to converge with a residual error of less than 10^{-3} and a corresponding total CPU runtime of 366 s using a 2.4-GHz processor. Without the preconditioner, the corresponding number of iterations and CPU runtime are, respectively, 323 iterations and 7217 s. The above calculations were also repeated for $w_x = 2.0$ μm, using a computational window with 90 and 82 sample points in the x and y directions, respectively. In this particular case, the preconditioned system requires ten iterations and 507 s to converge. Without the preconditioner, the corresponding numbers are 114 iterations and 3048 s. These results clearly demonstrate that the proposed preconditioner enhances the convergence rate of the numerical routine, which results in substantial reduction of CPU time requirements.

B. Channel Waveguide Suspended in Air

This waveguide has been selected due to its large transverse index discontinuity which presents a good test case for the present numerical method. As shown in Fig. 2(b), the core and cladding refractive indexes are assumed to be 3.6 and 1.0, respectively. The core thickness and the operating wavelength are fixed at 0.6 and 1.55 μm, respectively.

The calculated modal reflectivities are shown in Fig. 5 as a function of waveguide width w_x. The modal reflectivities based on the semi-vectorial and the full-vectorial models are in good agreement with each other when the waveguide width is relatively large. However, a large deviation of the prediction of the two models occurs when the waveguide width becomes small. For instance, based on full-vectorial model, the calculated modal reflectivity of the TE-Like mode is 0.385, at $w_x = 0.6$ μm (square waveguide). The corresponding value based on the semi-vectorial model is 0.22 which is much lower than the prediction of the full-vectorial model.

In order to ascertain the accuracy of our results, the incident power (P_i), the reflected power (P_r), and the transmitted power (P_t) at the waveguide facet were calculated. The variation of the power balance parameter, $\eta = \{(P_r + P_t)/P_i\} - 1$, with the waveguide core width is shown in Fig. 6. In the full-vectorial case, η remains low for all values of the waveguide width. However in the semi-vectorial case, the power balance parameter deteriorates when the waveguide width decreases below about 1.5 μm. The reason for the deterioration of the semi-vectorial model as the waveguide becomes narrow is straight forward to explain. It is well-known that when the waveguide decreases in width, the *minor* transverse field (H_x for the TE-like polarization and H_y for the TM-like polarization) becomes significant. Thus, the semi-vectorial model which ignores the minor field becomes inadequate and is expected to give inaccurate results leading to the poor power balance seen in Fig. 6.

In the case of the full-vectorial model which accounts for the minor field, η remains low ($<$0.002) irrespective of the waveguide width. It is noteworthy that throughout this work, η is maintained below 0.002 for all the reported full-vectorial results.

C. Raised Channel Waveguide

In the case of the raised channel waveguide shown in Fig. 2(c), the refractive indexes of the core and the substrate are assumed to be 3.6 and 3.4, respectively. The superstrate and the surrounding region is assumed to be air. The operating wavelength and core thickness are fixed at $\lambda = 1.55$ μm and $w_x = 0.9$ μm, respectively. Fig. 7 shows the modal reflectivity based on the semi-vectorial and full-vectorial models. The modal reflectivity in this case exhibits a similar behavior to that seen in the previous two waveguide structures. For a relatively large waveguide width, the modal reflectivities of the semi-vectorial and the full-vectorial cases are in good agreement with each other and they both tend to the results of the $2D$ model. In addition, the full-vectorial model is again seen to result in a higher model reflectivity compared to the semi-vectorial model when the waveguide width is reduced.

Fig. 8(a) and (b) shows the incident magnetic field components H_x and H_y, respectively, of the fundamental TE-Like

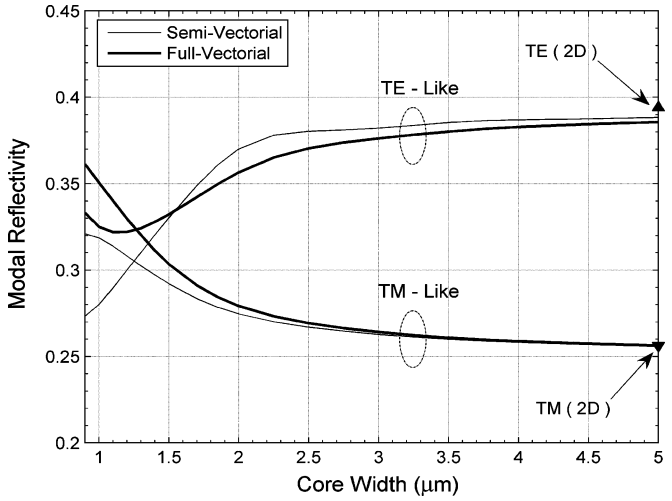

Fig. 7. Calculated TE-Like and TM-Like fundamental mode facet reflectivities corresponding to the waveguide structure shown in Fig. 2(c). The operating wavelength is $\lambda = 1.55\ \mu$m.

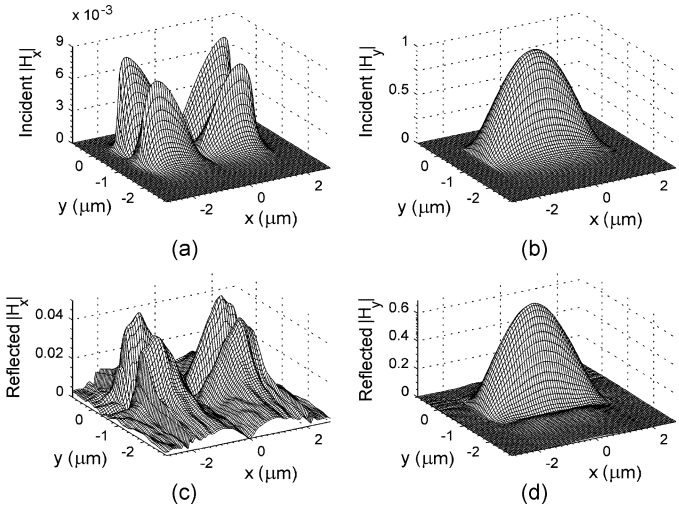

Fig. 8. Magnitude of the incident and reflected field components of the fundamental TE-Like mode for the waveguide structure shown in Fig. 2(c) for $w_x = 4\ \mu$m at $\lambda = 1.55\ \mu$m.

mode corresponding to the raised channel waveguide core width $w_x = 4\ \mu$m. It is seen that the incident minor field component H_x is very small compared to the incident major field component H_y. The reflected transverse magnetic field components are shown in Fig. 8(c) and (d). The reflected minor field component H_x remains low compared to the reflected major field component H_y. Thus, in this particular case, the minor field component may be ignored and hence the semi-vectorial and full-vectorial models should lead to similar values of the modal reflectivity.

Fig. 9(a)–(d) shows the corresponding field components of the fundamental TE-Like mode when the core width is reduced to $w_x = 1\ \mu$m. It is interesting to note that in this case, upon reflection; the minor field becomes substantial compared with the major field, as seen in Fig. 9(c) and (d), respectively. This result suggests an increase in the degree of polarization cross coupling, upon reflection, when the waveguide width is reduced. The semi-vectorial model, which ignores the presence of the

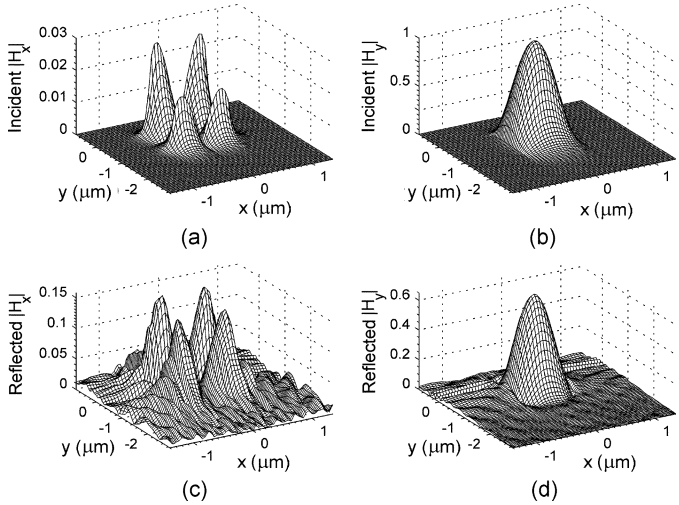

Fig. 9. Magnitude of the incident and reflected field components of the fundamental TE-Like mode for the waveguide structure shown in Fig. 2(c) for $w_x = 1\ \mu$m at $\lambda = 1.55\ \mu$m.

minor field, completely fails to account for this effect. This partially explains the discrepancy between the full-vectorial and the semi-vectorial results, seen in Fig. 7, when the waveguide width is reduced.

IV. Conclusion

A numerical approach for the treatment of abrupt waveguide discontinuities has been demonstrated. This approach is based on a 3-D full-vectorial formulation. It utilizes Padé approximants of the square root operator with branch cut rotation, which results in an efficient implementation. A rigorous boundary condition that accounts for all field components has been used in the numerical approach. In addition, a proposed preconditioner has been presented to reduce the number of iterations required for convergence of the numerical results. Application of the proposed approach to various waveguide facets exhibiting strong transverse and longitudinal discontinuities, show a substantial, and in some cases a large difference in the predictions of the semi-vectorial and the full-vectorial formulations when the waveguide width is reduced. For all waveguide structures studied, the predicted modal reflectivity based on the semi-vectorial formulation is less than that predicted by the full-vectorial model. Currently, work is being done to extend the present approach to account for multiple 3-D waveguide discontinuities based on the full-vectorial formulation.

References

[1] B. N. A. Rahman and J. B. Davies, "Analysis of optical waveguide discontinuities," *J. Lightw. Technol.*, vol. 6, no. 1, pp. 52–57, Jan. 1988.

[2] S. S. A. Obayya, "Novel finite element analysis of optical waveguide discontinuity problems," *J. Lightw. Technol.*, vol. 22, no. 5, pp. 1420–1425, May 2004.

[3] L. A. Vielva, J. A. Pereda, A. Vegas, and A. Prieto, "Simulating 3-D waveguide discontinuities using a combination of Prony's method and FDTD with improved absorbing boundary conditions," *Proc. Microw. Antennas Propagat.*, vol. 141, no. 2, pp. 127–132, Apr. 1994.

[4] N. Feng and W. Huang, "An efficient computation scheme for time-domain reflection at optical waveguide discontinuities," *IEEE Photon. Technol. Lett.*, vol. 16, no. 2, pp. 461–463, Feb. 2004.

[5] M. Reed, P. Sewell, T. M. Benson, and P. C. Kendall, "Efficient propagation algorithm for 3-D optical waveguides," *Proc. Optoelectron.*, vol. 145, no. 1, pp. 53–58, Feb. 1998.
[6] K. Jiang and W. P. Huang, "A finite-difference-based mode matching method for 3-D waveguide structures under semivectorial approximation," *J. Lightw. Technol.*, vol. 23, no. 12, pp. 4239–4248, Dec. 2005.
[7] G. Sztefka and H. P. Nolting, "Bidirectional eigenmode propagation for large refractive steps," *IEEE Photon. Technol. Lett.*, vol. 5, no. 5, pp. 554–557, May 1993.
[8] T. Rozzi, L. Zappelli, and M. N. Husain, "Radiation modes and step discontinuities in dielectric rib waveguide," *IEEE Trans. Microw. Theory Techn.*, vol. 40, no. 10, pp. 1879–1888, Oct. 1992.
[9] C. M. Herzinger, C. C. Lu, T. A. DeTemple, and W. C. Chew, "The semiconductor waveguide facet reflectivity problem," *IEEE J. Quantum Electron.*, vol. 29, no. 8, pp. 2273–2281, Aug. 1993.
[10] C. J. Smart, T. M. Benson, and P. C. Kendall, "Exact analysis of waveguide discontinuities: Junction and laser facets," *Electron. Lett.*, vol. 29, no. 15, pp. 1352–1353, Jul. 1993.
[11] U. Rogge and R. Pregla, "Method of lines for the analysis of dielectric waveguide," *J. Lightw. Technol.*, vol. LT-11, pp. 2015–2020, 1993.
[12] R. S. Burton and T. E. Schlesinger, "Least squares technique for improving three-dimensional dielectric waveguide analysis by the method of lines," *Electron. Lett.*, vol. 30, no. 13, pp. 1071–1072, Jun. 1994.
[13] J. Gerdes, S. Helfert, and R. Pregla, "Three-dimensional vectorial eigenmode algorithm for nonparaxial propagation in reflecting optical waveguide structures," *Electron. Lett.*, vol. 31, no. 1, pp. 65–66, Jan. 1995.
[14] Y. Chiou and H. Chang, "Analysis of optical waveguide discontinuities using the Padé approximants," *IEEE Photon. Technol. Lett.*, vol. 9, no. 7, pp. 964–966, Jul. 1997.
[15] H. El-Refaei, I. Betty, and D. Yevick, "The application of complex Padé approximants to reflection at optical waveguide facets," *IEEE Photon. Technol. Lett.*, vol. 12, no. 2, pp. 158–160, Feb. 2000.
[16] S. H. Wei and Y. Y. Lu, "Application of Bi-CGSTAB to waveguide discontinuity problems," *IEEE Photon. Technol. Lett.*, vol. 14, no. 5, pp. 645–647, May 2002.
[17] H. Rao, R. Scarmozzino, and R. M. Osgood, Jr., "A bidirectional beam propagation method for multiple dielectric interfaces," *IEEE Photon. Technol. Lett.*, vol. 11, no. 7, pp. 830–832, Jul. 1999.
[18] H. Rao, M. J. Steel, R. Scarmozzino, and R. M. Osgood, Jr., "Complex propagators for evanescent waves in bidirectional beam propagation method," *J. Lightw. Technol.*, vol. 18, no. 8, pp. 1155–1160, Aug. 2000.
[19] H. El-Refaei, D. Yevick, and I. Betty, "Stable and noniterative bidirectional beam propagation method," *IEEE Photon. Technol. Lett.*, vol. 12, no. 4, pp. 389–391, Apr. 2000.
[20] P. L. Ho and Y. Y. Lu, "A stable bidirectional propagation method based on scattering operators," *IEEE Photon. Technol. Lett.*, vol. 13, no. 12, pp. 1316–1318, Dec. 2001.
[21] Y. Y. Lu and S. H. Wei, "A new iterative bidirectional beam propagation method," *IEEE Photon. Technol. Lett.*, vol. 14, no. 11, pp. 1533–1535, Nov. 2002.
[22] K. Kawano, T. Kitoh, M. Kohtoku, T. Takeshita, and Y. Hasumi, "3-D semivectorial analysis to calculate facet reflectivities of semiconductor optical waveguides based on the Bi-directional method of line BPM (MoL-BPM)," *IEEE Photon. Technol. Lett.*, vol. 10, no. 1, pp. 108–110, Jan. 1998.
[23] N. N. Feng and W. P. Huang, "A field-based numerical method for three-dimensional analysis of optical waveguide discontinuities," *IEEE J. Quantum Electron.*, vol. 39, no. 12, pp. 1661–1665, Dec. 2003.
[24] K. Bierwirth, N. Schultz, and F. Arndt, "Finite-difference analysis of rectangular dielectric waveguide structures," *IEEE Trans. Microw. Theory Techn.*, vol. 34, pp. 1104–1113, 1986.
[25] P. Lusse, P. Stuwe, J. Schule, and H. G. Unger, "Analysis of vectorial mode fields in optical waveguides by a new finite difference method," *J. Lightw. Technol.*, vol. 12, no. 3, pp. 487–494, Mar. 1994.
[26] N. N. Feng, C. Xu, W. P. Huang, and D. G. Fang, "A new preconditioner based on paraxial approximation for stable and efficient reflective beam propagation method," *J. Lightw. Technol.*, vol. 21, no. 9, pp. 1996–2001, Sep. 2003.
[27] H. A. Jamid, "Enhanced PML performance using higher order approximation," *IEEE Trans. Microw. Theory Techn.*, vol. 52, no. 4, pp. 1166–1174, Apr. 2004.

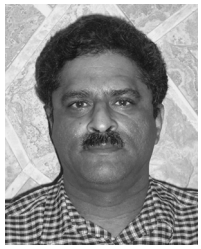

Husain A. Jamid received the B.S. and M.S. degrees from Arizona State University, Tempe, AZ, in 1981 and 1983, respectively, and the Ph.D. degree from King Fahd University of Petroleum and Minerals (KFUPM), Dhahran, Saudi Arabia, in 1986, all in electrical engineering.

He is currently a Professor with the Electrical Engineering Department, KFUPM. He has done research work in metal-clad as well as nonlinear optical waveguides. His current research interest is in optical device simulation and development of related numerical methods.

Dr. Jamid has received the KFUPM Excellence in Teaching Award three times. Since July 2005, he has been the Electrical Engineering Subject Editor for the *Arabian Journal for Science and Engineering*.

Md. Zahed M. Khan was born in Hyderabad, India. He received the B.E. degree in electronics and communication from Osmania University, Hyderabad, India, in 2001 and the M.S. degree in electrical engineering from King Fahd University of Petroleum and Minerals (KFUPM), Dhahran, Saudi Arabia, in 2004.

He worked as a Lecturer in Shadan College of Engineering and Technology, affiliated with Jawaharlal Nehru Technological University, Hyderabad, India, in 2001–2002. During his course of study in the Electrical Engineering Department, KFUPM, he was a Research Assistant engaged in teaching and research activities. Since 2004, he has been with the Electrical and Electronics Engineering Technology Department of Hafr Al-Batin Community College, KFUPM, where he is currently a Lecturer. His current area of research is the analysis of 3-D optical waveguide problems. His main area of interest includes numerical analysis of integrated optical waveguide structures, optical communication, and digital electronics.